Stochastic Unit Commitment in Low-Inertia Grids

Matthieu Paturet, Uros Markovic, *Member, IEEE*, Stefanos Delikaraoglou, *Member, IEEE*, Evangelos Vrettos, *Member, IEEE*, Petros Aristidou, *Senior Member, IEEE*, and Gabriela Hug, *Senior Member, IEEE*

***Abstract*—In this paper, the Unit Commitment (UC) problem in a power network with low levels of rotational inertia is studied. Frequency-related constraints, namely the limitation on Rate-of-Change-of-Frequency (RoCoF), frequency nadir and steady-state frequency error, are derived from a uniform system frequency response model that incorporates dynamics and controls of both synchronous generators and grid-forming inverters. These constraints are then included into a stochastic UC formulation that accounts for wind power and equipment contingency uncertainties using a scenario-tree approach. In contrast to the linear RoCoF and steady-state frequency error constraints, the nadir constraint is highly nonlinear. To preserve the mixed-integer linear formulation of the stochastic UC model, we propose a computationally efficient approach that allows to recast the nadir constraint by introducing appropriate bounds on relevant decision variables of the UC model. This method is shown to be generally more accurate and computationally more efficient for medium-sized networks than a piece-wise linearization method adapted from the literature. Simulation results for a modified IEEE RTS-96 system revealed that the inclusion of inertia-related constraints significantly influences the UC decisions and increases total costs, as more synchronous machines are forced to be online to provide inertial response.**

***Index Terms*—Unit commitment, low-inertia grid, frequency constraints, wind uncertainty, voltage source converter.**

NOMENCLATURE

The main notation used for the unit commitment problem formulation in this paper is introduced below. Additional symbols are defined in the paper where needed. All symbols are augmented by index t when referring to different time periods.

A. Sets and Indices

$\ell \in \mathcal{L}$	Set of transmission lines.
$\xi \in \mathcal{E}$	Set of scenarios $\xi = \{c, \omega\}$ including generation outages (c) and wind power uncertainty (ω).
$i \in \mathcal{I}$	Set of conventional generation units.
$j \in \mathcal{J}$	Set of converter-interfaced (i.e., wind) generation units.
$d \in \mathcal{J}_d$	Subset of converter-interfaced generation units providing droop control.
$v \in \mathcal{J}_v$	Subset of converter-interfaced generation units providing virtual inertia.
$n \in \mathcal{N}$	Set of nodes.
$\mathcal{I}_n$	Set of conventional generation units located at bus n.
$\mathcal{J}_n$	Set of converter-based units located at bus n.

B. Decision variables

$\hat{\delta}_n$	Day-ahead voltage angle at node n [rad].
$\tilde{\delta}_{n\xi}$	Real-time voltage angle at node n in scenario ξ [rad].
$F_{\xi t}$	Fraction of total power generated by high-pressure turbines in scenario ξ [p.u.].
$k_{i\xi t}$	Scaled power gain factor of conventional generator i in scenario ξ [p.u.].
$l^{\text{shed}}_{n\xi t}$	Shedding of load at node n in scenario ξ [MW].
$M_{\xi t}$	Aggregate inertia constant of conventional generators in scenario ξ [s].
$D_{\xi t}$	Aggregate damping constant of conventional generators in scenario ξ [p.u.].
p_{it}	Day-ahead dispatch of conventional generator i [MW].
$r^{+/-}_{i\xi t}$	Up/Downward reserve deployment of generator i in scenario ξ [MW].
$R_{\xi t}$	Aggregate droop factor of conventional generators in scenario ξ [p.u.].
u_{it}	Commitment status of conventional generator i.
w_{jt}	Day-ahead dispatch of wind generator j [MW].
$w^{\text{spill}}_{j\xi t}$	Wind spillage of generator j in scenario ξ [MW].
y_{it}	Start-up variable of conventional generator i.
z_{it}	Shut-down variable of conventional generator i.

C. Parameters

M_i	Inertia constant of conventional generator i [s].
D_i	Damping constant of conventional generator i [p.u.].
R_i	Droop gain of conventional generator i [p.u.].
K_i	Mechanical power gain of conventional generator i [p.u.].
F_i	Fraction of total power generated by the turbine of conventional generator i [p.u.].
M_v	Virtual inertia constant of converter-based generator v [s].

Manuscript received April 4, 2019; revised September 3, 2019, December 13, 2019, and March 11, 2020; accepted March 29, 2020. Date of publication April 13, 2020; date of current version August 24, 2020. Paper no. TPWRS-00490-2019. *(Corresponding author: Uros Markovic.)*

Matthieu Paturet, Uros Markovic, and Gabriela Hug are with the Power Systems Laboratory, ETH Zurich, 8092 Zürich, Switzerland (e-mail: matthieu.paturet@gmail.com; markovic@eeh.ee.ethz.ch; ghug@ethz.ch).

Stefanos Delikaraoglou is with the Laboratory for Information and Decision Systems, MIT, Cambridge, MA 02139 USA (e-mail: sdelikar@mit.edu).

Evangelos Vrettos is with the Swiss Electricity Transmission System Operator, 5001 Aarau, Switzerland (e-mail: evangelos.vrettos@swissgrid.ch).

Petros Aristidou is with the Department of Electrical Engineering and Computer Engineering and Informatics, Cyprus University of Technology, limassol 3036, Cyprus (e-mail: p.aristidou@ieee.org).

Color versions of one or more of the figures in this article are available online at https://ieeexplore.ieee.org.

Digital Object Identifier 10.1109/TPWRS.2020.2987076

D_v	Virtual damping constant of converter-based generator v [p.u.].
R_d	Droop gain of converter-based generator d [p.u.].
$\alpha_{i\xi t}$	Outage parameter of conventional generator i in scenario ξ.
$\Delta P_{\xi t}$	Size of power outage in scenario ξ [p.u.].
π_ξ	Probability of occurrence of scenario ξ.
B_{nm}	Susceptance of transmission line (n, m) [S].
C_i	Day-ahead price offer of generator i [\$/MWh].
$C_i^{\mathrm{SU/SD}}$	Start-up/Shut-down price offer of generator i [\$].
$C_i^{+/-}$	Up/Downward reserve price offer of generator i [\$/MWh].
C^{sh}	Value of lost load [\$/MWh].
$\underline{L}_{nt}$	Load demand at node n [MW].
$\overline{f}_{nm}$	Capacity of transmission line (n, m) [MW].
$\overline{P}_i/\underline{P}_i$	Active power limits of conventional generator i [MW].
$R_i^{+/-}$	Up/Downward reserve capacity of generator i [MW].
$R_i^{\mathrm{U/D}}$	Ramp up/down limits of conventional generator i [MW/h].
$W^*_{j\xi t}$	Wind power realization of generator j in scenario ξ [MW].
W_d	Total power capacity of converter-interfaced generators providing droop control [MW].
W_v	Total power capacity of converter-interfaced generators providing virtual inertia [MW].

I. Introduction

With increasing penetration of Renewable Energy Sources (RES), system operators face new challenges in order to ensure power grid stability. One of these challenges is frequency stability due to a loss of generation or a large variation of load. In traditional power systems, synchronous generators (e.g., hydro or steam turbines) provide rotational inertia through stored kinetic energy in their rotating mass (turbine system and rotor). This energy is important to stabilize the system as it ensures slower frequency dynamics and reduces the Rate-of-Change-of-Frequency (RoCoF) in case of a generation-demand imbalance [1]. In the future, with more generation coming from wind and solar power, the ability of the system to maintain frequency within the acceptable range is diminished. Indeed, photovoltaic systems are connected to the grid through inverters, which do not exhibit rotational inertia. Even in the case of inverter-interfaced wind generators, the inverter electrically decouples the rotor's rotational inertia from the system [2].

Transmission System Operators (TSOs) around the world are concerned with the stability issues associated with large penetration of renewable energy in their systems. In the United States, the Electric Reliability Council of Texas (ERCOT) has studied the effect of low-inertia on the security and reliability of the grid [3]. As the system inertia at ERCOT continues to decrease with the growth of wind generation, multiple technical solutions have been explored to mitigate the adverse impact on frequency control performance. Most notably, bringing more synchronous inertia online by committing additional units, committing different units that have higher inertia, or using synchronous condensers, as well as slowing down the RoCoF after an event (e.g., generator trip) by increasing the rate of primary frequency response of the system. Moreover, ERCOT has recently altered the methodology for determining Responsive Reserve Service (RRS) from procuring a constant reserve for all hours to determining necessary amounts of RRS dynamically based on expected system inertia conditions. On the other hand, the Irish TSO (EirGrid) is designing new ancillary services to remunerate providers of rotational or synthetic inertia [4], [5]. EirGrid also currently imposes limits on the maximum instantaneous penetration of variable RES with respect to the total load demand at any point in time.

In systems with low rotational inertia, TSOs must impose minimum inertia requirements in order to secure frequency stability and avoid system collapse in case of a severe fault or a sudden mismatch between generation and demand. With such new requirements, the traditional Unit Commitment (UC) problem, i.e., the day-ahead scheduling process to decide which generators will be committed, may be affected as more Synchronous Generators (SGs) could be dispatched for the sole purpose of providing inertia. Nonetheless, the ex-ante definition of inertia and reserve requirements to cope with the sudden deviations from generation outages and renewables' forecast errors, respectively, is a challenging task due to the uncertain nature of these imbalances. To this end, this work adopts a stochastic version of the UC problem that can endogenously account for the aforementioned uncertainty sources via a set of scenarios that model plausible equipment contingencies and renewables' forecast errors. In turn, this model can pre-position the flexible system resources at the day-ahead stage, without resorting to deterministic reserve requirements, in a way that improves the response to the real-time variations and minimizes the expected system cost.

Several papers have approached the problem of including inertia requirements in the UC problem. In [6]–[8], the authors use the swing equation of Center-of-Inertia (CoI), which allows them to derive a RoCoF constraint and study its effect on the UC schedule. However, this approach oversimplifies the problem as it neglects metrics related to frequency deviation from the setpoint. This problem was addressed in [9]–[13] with the inclusion of a constraint limiting the post-disturbance maximum frequency deviation (i.e., frequency nadir). In [9], the analytic form of frequency nadir as a function of active power disturbance is derived using a system frequency model obtained from [14]. The nadir expression is then linearized and added to the UC model, while considering a fixed sudden load increase. On the other hand, the studies in [10]–[13] bypass the explicit modeling of turbine and governor control as well as their impact on frequency dynamics by imposing strict assumptions on system damping and total frequency response provision at each node. Moreover, the primary frequency response provision by SGs (essentially droop control) is approximated as a constant ramp function of time in order to decouple the governor control from frequency and simplify the analytical formulation of the problem. In addition, [13] optimizes the energy production and multi-speed allocation of frequency response services,

whereas [10] looks at the impact of wind uncertainty on inertia requirements. While the proposed simplifications enable the inclusion of a nadir constraint without the explicit consideration of second-order frequency dynamics, they oversimplify the actual control implementation and disregard the aggregate impact of governor damping. Furthermore, none of the aforementioned studies incorporates the converter interface of RES and the impact of respective control schemes on the UC formulation.

The contributions of this paper are threefold. First, we improve the frequency dynamics model in [9] by including the state-of-the-art converter control schemes of inverter-based generation, more specifically Virtual Synchronous Machine (VSM) and droop control. In contrast to the existing literature, where SG inertia and damping constants are usually numerically modified in order to compensate for high RES integration, we analyze a realistic model of a low-inertia system comprising both SG and converter dynamic models. This allows us to derive detailed analytic expressions of relevant frequency metrics as functions of multiple system variables (e.g., inertia, damping, aggregate droop gain, etc.) to be determined by the UC model, as opposed to the approach in [10] where the inertia constant was the only decision variable of interest. Moreover, in addition to frequency nadir and RoCoF, the limitation on Quasi Steady-State (QSS) frequency deviation is incorporated into the UC formulation. No prior work considers the dynamics and controls of virtual inertia units in the derivation of frequency constraints for inclusion in UC and hence this is the main contribution of the paper. Secondly, a more straightforward method is proposed to extract bounds for decision variables contributing to frequency nadir, which allows us to incorporate the non-linear nadir constraint in the UC problem in a more accurate way compared to [9], while at the same time reducing the computational burden for mid-sized systems. Finally, similar to [10], this paper includes both the wind uncertainty and potential loss of generation in the UC model. However, this work presents a more comprehensive approach towards event probability computation and structuring of the scenario tree for the two-stage stochastic UC problem.

The rest of the paper is structured as follows. In Section II, the derivation of post-contingency frequency dynamics in a low-inertia, multi-machine system is discussed. The obtained time-domain, analytic expressions are then incorporated into a stochastic UC formulation in Section III, after linearizing the initially non-linear frequency nadir constraint. Subsequently, the modeling of uncertainties, namely equipment failure and wind power, in the form of probabilistic scenarios is presented in Section IV. Section V provides the mathematical formulation of the stochastic UC problem. Finally, Section VI presents and discusses the simulation results using a modified version of the IEEE RTS-96 system, whereas Section VII draws the main conclusions and discusses the outlook of the study.

II. Low-Inertia System Frequency Dynamics

A. Inertial Response and Primary Frequency Control Model

We first focus on deriving a simplified, but sufficiently accurate, uniform frequency response model of a low-inertia system previously introduced in [15]. Let us consider a system

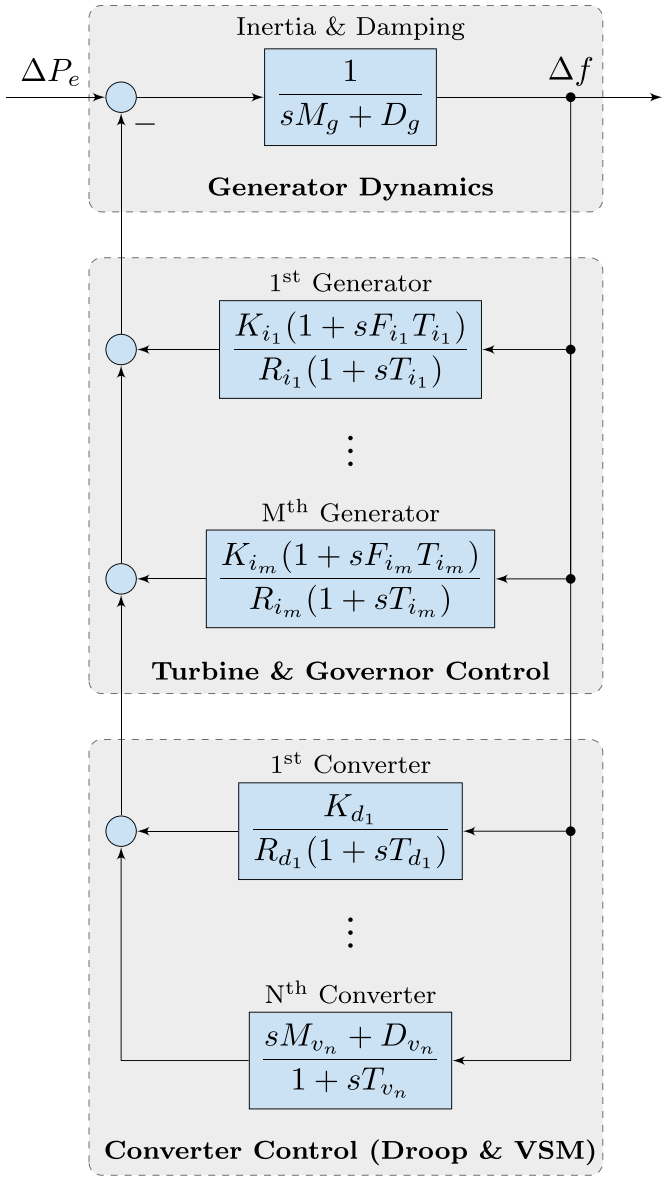

Fig. 1. Uniform system frequency dynamics model.

comprised of *traditional* ($i \in \mathcal{I}$) and *converter-based* ($j \in \mathcal{J}$) generators depicted in Fig. 1.

The generator dynamics are described by the swing equation, with M_g and D_g denoting the normalized inertia and damping constants corresponding to the synchronous generators' CoI. The low-order model proposed in [16] is used for modeling the governor droop and turbine dynamics; T_i are the turbine time constants, R_i and K_i are the respective droop and mechanical power gain factors, while F_i refers to the fraction of total power generated by the turbines of synchronous machines. Furthermore, we incorporate the impact of grid-forming converters, as they are the only type of power electronic-interfaced units providing frequency support [17], [18]. A particular focus is set on droop ($d \in \mathcal{J}_d \subseteq \mathcal{J}$) and VSM ($v \in \mathcal{J}_v \subseteq \mathcal{J}$) control schemes, as two of the currently most prevalent emulation techniques in the literature, which in fact have equivalent properties in the

grid-forming mode of operation [19]. Here, $T_d = T_v \equiv T_j$ are the time constants of all converters, R_d and K_d are the respective droop and electrical power gain factors, whereas M_v and D_v denote the normalized virtual inertia and damping constants of VSM converters.

B. Analytic Derivation of Frequency Metrics

From Fig. 1, a transfer function $G(s)$ of a general-order system dynamics can be derived, as follows:

$$G(s) = \frac{\Delta f}{\Delta P_e} = \Bigg(\underbrace{(sM_i + D_i) + \sum_{i\in\mathcal{I}} \frac{K_i(1+sF_iT_i)}{R_i(1+sT_i)}}_{\text{traditional generators}} + \underbrace{\sum_{d\in\mathcal{J}_d} \frac{K_d}{R_d(1+sT_d)}}_{\text{droop converters}} + \underbrace{\sum_{v\in\mathcal{J}_v} \frac{sM_v + D_v}{1+sT_v}}_{\text{VSM converters}} \Bigg)^{-1}. \quad (1)$$

Assuming similar time constants ($T_i \approx T$) of all synchronous machines, usually 2-3 orders of magnitude higher than the ones of converters, justifies the approximation $T \gg T_j \approx 0$. Now (1) is transformed into the following expression:

$$G(s) = \frac{1}{MT} \frac{1+sT}{s^2 + 2\zeta\omega_n s + \omega_n^2}, \quad (2)$$

where the natural frequency (ω_n) and damping ratio (ζ) are

$$\omega_n = \sqrt{\frac{D+R_g}{MT}}, \quad \zeta = \frac{M + T(D+F_g)}{2\sqrt{MT(D+R_g)}}, \quad (3)$$

and parameters (M, D) and (F_g, R_g) represent weighted system and synchronous generator averages, respectively. More details on mathematical formulation can be found in [15].

Assuming a stepwise disturbance in the electrical power $\Delta P_e(s) = -\Delta P/s$, we can derive the time-domain expression for frequency deviation as well as the nadir ($\dot{f}_{\max}$), RoCoF ($\dot{f}_{\max}$) and steady-state deviation ($\Delta f_{\rm ss}$) frequency metrics:

$$\Delta f_{\max} = -\frac{\Delta P}{D+R_g}\left(1 + \sqrt{\frac{T(R_g-F_g)}{M}} e^{-\zeta\omega_n t_m}\right), \quad (4a)$$

$$\dot{f}_{\max} = \dot{f}(t_0^+) = -\frac{\Delta P}{M}, \quad (4b)$$

$$\Delta f_{\rm ss} = -\frac{\Delta P}{D+R_g}, \quad (4c)$$

with $t_m = \frac{1}{\omega_d}\tan^{-1}(\frac{\omega_d}{\zeta\omega_n - T^{-1}})$ being the time instance of frequency nadir and $\omega_d = \omega_n\sqrt{1-\zeta^2}$.

The accuracy of the proposed model has already been investigated and verified in [15]. We can conclude that the frequency metrics of interest are directly dependent on the average system parameters M, D, R_g and F_g, and thus they could be regulated through the UC model. In particular, RoCoF and steady-state deviation can be explicitly controlled via $\dot{f}_{\max} \sim M^{-1}$ and $\Delta f_{\rm ss} \sim (D+R_g)^{-1}$, while nadir can be modeled using a highly non-linear function $\Delta f_{\max}(M, D, R_g, F_g)$. Therefore, by incorporating the frequency metrics in the UC problem, it is possible to make day-ahead generator commitment decisions that ensure satisfactory real-time frequency response in case of outages.

III. Formulation of Frequency Constraints

The aforementioned frequency expressions in (4) are incorporated as constraints into the stochastic UC problem, converted into SI and bounded by prescribed ENTSO-E (European Network of Transmission System Operators for Electricity) thresholds [20], as follows:

$$\left|\frac{f_b\Delta P}{D+R_g}\left(1 + \sqrt{\frac{T(R_g-F_g)}{M}} e^{-\zeta\omega_n t_m}\right)\right| \leq \Delta f_{\rm lim}, \quad (5a)$$

$$\left|\frac{f_b\Delta P}{M}\right| \leq \dot{f}_{\rm lim}, \quad (5b)$$

$$\left|\frac{f_b\Delta P}{D+R_g}\right| \leq \Delta f_{\rm ss,lim}, \quad (5c)$$

with $f_b = 50\,\text{Hz}$ being the base frequency; $\Delta f_{\rm lim} = 0.4\,\text{Hz}$ is the Under-Frequency Load Shedding (UFLS) trigger, while $\dot{f}_{\rm lim} = 0.5\,\text{Hz/s}$ and $\Delta f_{\rm ss,lim} = 0.2\,\text{Hz}$ are the maximum permissible RoCoF and steady-state frequency deviation.

Constraints (5b) and (5c) are linear, unlike the non-linear frequency nadir constraint (5a). In order to avoid the high computational burden of a Mixed-Integer Non-Linear Program (MINLP) formulation and have a measurable optimality gap, a linear approximation of (5a) is used which allows us to maintain a Mixed-Ineger Linear Program (MILP) formulation of the stochastic UC problem. By integrating (5a)-(5c) in the UC problem, we are able to capture the system's real-time dynamic boundary conditions already in the day-ahead UC scheduling phase in a way that improves frequency response and minimizes the risk of load shedding.

A. Piece-Wise Linearization of Nadir Expression

The study in [9] proposes a Piece-Wise Linearization (PWL) technique for obtaining a linearized expression for frequency nadir in order to subsequently integrate it into a UC problem. To improve clarity, this technique is outlined here before comparing its computational burden against our proposed approach introduced in Section III-B. Let us recall from Section II-B that the frequency nadir expression is a function of four variables (R_g, F_g, M, D), and as such too complicated to be directly handled by the PWL. Considering that the aggregate damping constant is of the form $D(D_i, D_v, R_d)$, with respective damping and droop gains usually strictly prescribed within narrow ranges by the system operator, it is justifiable to assume a constant D. Therefore, the frequency nadir becomes a function of three variables, i.e., $\Delta f_{\max}(M, R_g, F_g)$. Hence, the PWL formulation aims to minimize the following objective function

$$\min_{\Psi} \sum_{\eta} \Bigg(\max_{1\leq\nu\leq\bar{\nu}} \left\{ a_\nu R_g^{(\eta)} + b_\nu F_g^{(\eta)} + c_\nu M^{(\eta)} + d_\nu \right\} - \Delta f_{\max}\left(R_g^{(\eta)}, F_g^{(\eta)}, M^{(\eta)}\right) \Bigg)^2, \quad (6)$$

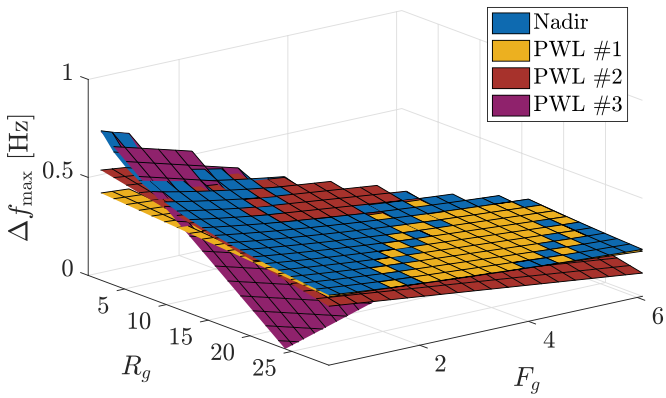

Fig. 2. PWL of the nadir constraint for $M = 9$.

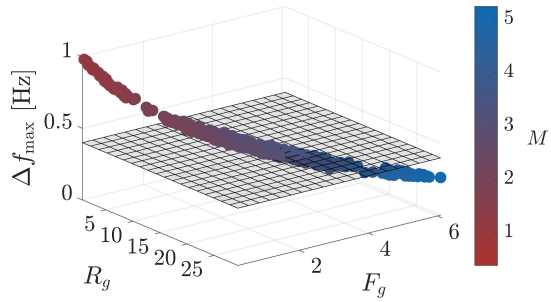

Fig. 3. All possible values of the nadir after a generator loss.

TABLE I
COMPUTATIONAL COST OF THE LINEARIZATION METHODS

Linearization technique	Computational time [s]
PWL ($\eta = 3, \nu = 4$)	70
PWL ($\eta = 4, \nu = 4$)	7200
Bound extraction	20

with $\Psi = \{a_\nu, b_\nu, c_\nu, d_\nu, \forall \nu\}$, being the set of optimization variables, η denoting the evaluation point and ν referring to the number of PWL segments. The objective function (6) penalizes the difference between the appropriate PWL segment and the nadir function at all evaluation points. Given the convex nature of the nadir function, the inner max operator chooses the appropriate PWL segment for each evaluation point by looking at which segment is closest to the curve at that specific point. To improve understanding, we elaborate on the mathematical formulation and the practical implementation of the PWL from [9] in Appendix A.

Upon obtaining the optimal solution of the model in (6), denoted as $(a^*_\nu, b^*_\nu, c^*_\nu, d^*_\nu)$, the nadir constraint can be integrated into the MILP UC model by adding a set of inequalities, along with the nadir threshold constraint of the form $f_b\, t_3 \leq \Delta f_{\lim}$. The results for the approximation of frequency nadir function for a test system of 20 generators described in Section VI are shown in Fig. 2, where a loss of the largest unit is considered. Note that Fig. 2 showcases the surface plot for a fixed inertia constant M and thus ignores one degree of freedom. The original surface is presented in blue, whereas its PWL-approximation segments are the planes depicted in various colors. It is important to note that the optimization problem (6) is computationally intensive and thus in order to obtain results within reasonable computational time, the number of PWL segments used for the approximation as well as the number of evaluation points have to be kept low.

B. Extracting Bounds on Relevant Variables

An alternative approach for linearizing the nadir constraint and integrating it into the UC problem is to confine the values of R_g, F_g, M and D within a plausible range to guarantee that the nadir threshold in (5a) is not violated. With this approach the damping variable D can easily be included and does not need to be set constant. The scatter plot presented in Fig. 3 reflects all possible values of frequency nadir after the loss of the largest generator, for the same system as in Section III-A. In the general case, for a system that comprises $|\mathcal{I}|$ generators, there will be $2^{|\mathcal{I}|-1}$ possible generator commitment combinations after a generator outage. By obtaining the set of these dispatch combinations, the values of R_g, F_g, M and D at which the UFLS threshold is not violated can be extracted, corresponding to the points below the shaded plane in Fig. 3. Subsequently, these values are used to substitute the nadir constraint in the unit commitment as follows:

$$F_g \geq F_g^{\lim}, \quad R_g \geq R_g^{\lim}, \quad M \geq M^{\lim}, \quad D \geq D^{\lim}. \quad (7)$$

The proposed method provides increased accuracy for the introduction of frequency nadir as a constraint in the UC problem. Indeed, as every possible generator combination is calculated after the loss of any single generator in the system, the exact values of frequency nadir are known and thus the constraint will not introduce any error in the optimization.

Table I provides a comparison of the proposed method to the PWL technique in terms of computational time that is needed to obtain the equivalent linear nadir expression for a single value of ΔP. It is clear that the PWL is more time intensive, especially when aiming for an increased precision. In fact, running the PWL method with more than 4 evaluation points and 4 linear segments was not computationally possible using a standard laptop computer. It should be noted though that for very large systems, the calculations of $2^{|\mathcal{I}|-1}$ combinations for the bound extraction method would become more computationally expensive, as the computation time increases by a factor of $2^{\Delta|\mathcal{I}|}$ for every additional $\Delta|\mathcal{I}|$ generators included in the system.

Nevertheless, the computational effort of the bounds extraction method could be drastically reduced through certain simplifications, therefore making it tractable on a larger scale. For instance, many combinations of committed generation could be immediately discarded if they do not meet prescribed RoCoF limits at the instance of the disturbance. In particular, one should consider only the system dispatch with aggregate inertia above $M_{\min} = |\Delta P|/\dot{f}_{\lim}$, which could easily be incorporated into the bound extraction scheme. It should also be noted that the computational burden arises solely from the sheer number of all possible generation commitment schedules, and the calculation

of frequency nadir for each individual scenario can be done independently. Therefore, parallelization techniques can be readily employed to speed up the overall computation and improve the tractability of the proposed approach.

For the purposes of this paper, the proposed bound extraction method will be used as it is significantly faster and introduces less error when applied to the 20-generator test system under investigation.

IV. Modeling Equipment-Failure and Wind Power Uncertainties

This section describes the modeling of uncertainty pertaining to equipment failure and wind power production during power system operation. The uncertain nature of wind power production is modeled using a set of scenarios $\mathcal{W}$ that captures the spatio-temporal interdependence of forecast errors, for every wind farm location and during the whole scheduling horizon. Each wind power realization scenario $\omega \in \mathcal{W}$ has the same probability of occurrence denoted by π_ω.

In terms of equipment failure uncertainty, this work considers as the set of credible contingencies the unforeseen outages of synchronous generators, whereas transmission assets are assumed to be $100\,\%$ reliable. In order to reduce the computational burden, we follow the assumption from [21] considering that the generation outages happen at a discrete time period, while failed assets remain unavailable for the rest of the scheduling horizon, i.e., the Mean Time To Repair (MTTR) is greater than the scheduling horizon of the day-ahead electricity market. For the purpose of assessing the impact of frequency constraints on the unit commitment schedule, we consider as contingency period the one in which the power system faces the highest wind power penetration as scarcity of inertia is most likely to occur in this time due to the displacement of synchronous generators from the day-ahead schedule.

To calculate the probability π_c associated with contingency scenario c, we index the set of credible contingencies by $\kappa = 1, 2, \ldots, \mathcal{K}$. $A(\kappa, \tau)$ denotes the random event of contingency κ happening within time period τ. Random event $B(\kappa)$ corresponds to contingency κ not occurring during the entire scheduling horizon. We further denote as λ_κ the inverse of the Mean Time To Failure (MTTF) κ, i.e., $\lambda_\kappa = 1/\mathrm{MTTF}$. Considering that we are looking at only one hour in which the outages may occur and assuming that the time between two consecutive equipment failures follows an exponential distribution [22], the probability π_c for each contingency scenario κ is derived from the probabilities of occurrence of random events $A(\kappa, \tau)$ and $B(\kappa)$ that are calculated using the following expressions according to [23]:

$$\pi[A(1,\tau)] = \exp(-\lambda_1\tau)(\exp(\lambda_1)-1), \tag{8a}$$

$$\pi[A(1,\tau)] = \pi[A(2,\tau)] = \ldots = \pi[A(\mathcal{K},\tau)], \tag{8b}$$

$$\pi[B(1)] = \exp(-\lambda_1\tau), \tag{8c}$$

$$\pi[B(1)] = \pi[B(2)] = \ldots = \pi[B(\mathcal{K})]. \tag{8d}$$

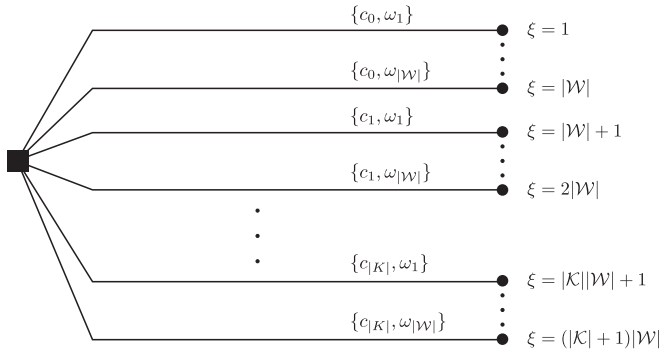

Fig. 4. Scenario tree for the two-stage stochastic UC problem.

Assuming statistical independence between all contingencies, the probability π_{c_0} of the no-contingency scenario is equal to

$$\pi_{c_0} = \prod_{\kappa=1}^{\mathcal{K}} \pi[B(\kappa)], \tag{9}$$

while the probability π_{c_κ} of losing a generator is equal to

$$\pi_{c_\kappa} = \pi[A(1,\tau)] \prod_{\substack{y=1 \\ y\neq k}}^{\mathcal{K}} \pi[B(y)], \quad \forall \kappa = 1, ..., \mathcal{K}. \tag{10}$$

It should be noted that the sum of probabilities π_{c_0} and π_{c_κ} is lower than 1, since sequential contingencies are not considered. For instance, setting MTTF equal to $1000\,\mathrm{h}$ for all generators, we obtain from (8) $\pi[A(\kappa,\tau)] = 0.9995 \times 10^{-3}$ and $\pi[B(\kappa)] = 0.9990$. According to (9) and (10) we obtain respectively $\pi_{c_0} = 0.9960$ and $\pi_{c_\kappa} = 0.9965 \times 10^{-3}$ and thus $\sum_{\kappa=0}^{4} \pi_{c_\kappa} = 0.9999 \approx 1$.

Combining the scenarios modeling the equipment failure and wind power uncertainty into a single scenario set $\mathcal{E}$, each scenario ξ is defined as a pair of contingency c and wind power realization ω. For each $\xi = \{c, \omega\}$ the corresponding probability of occurrence is given as $\pi_\xi = \pi_\omega \cdot \pi_c$ and $\sum_{\xi\in\mathcal{E}} \pi_\xi \approx 1$, assuming that equipment outages and wind power production are statistically independent events. The structure of the scenario set $\mathcal{E}$ used in the stochastic UC formulation is illustrated as the scenario tree shown in Fig. 4, for $|\mathcal{K}|$ contingencies and $|\mathcal{W}|$ wind power scenarios.

V. Stochastic Unit Commitment

This section provides the mathematical formulation of the stochastic unit commitment [24], with the addition of frequency-related constraints. The proposed model is a two-stage stochastic optimization problem of the form:

$$\min_{\Phi} \sum_{t\in\mathcal{T}} \sum_{i\in\mathcal{I}} \left(C_i^{\mathrm{SU}} y_{it} + C_i^{\mathrm{SD}} z_{it} + C_i p_{it}\right) + \sum_{t\in\mathcal{T}} \sum_{\xi\in\mathcal{E}} \pi_\xi \left[\sum_{i\in\mathcal{I}} \left(C_i^{+} r_{i\xi t}^{+} - C_i^{-} r_{i\xi t}^{-}\right) + \sum_{n\in\mathcal{N}} C^{\mathrm{sh}}\, l_{n\xi t}^{\mathrm{shed}}\right] \tag{11a}$$

subject to

$$\sum_{i\in\mathcal{I}_n} p_{it} + \sum_{j\in\mathcal{J}_n} w_{jt} - L_{nt} - \sum_{m:(n,m)\in\mathcal{L}} B_{nm}(\delta_{nt}-\delta_{mt}) = 0, \quad \forall n,t, \tag{11b}$$

$$B_{nm}(\delta_{nt}-\delta_{mt}) \le \overline{f}_{nm}, \quad \forall (n,m)\in\mathcal{L}, t, \tag{11c}$$

$$u_{it} - u_{i(t-1)} \le u_{i\tau_i^1}, \quad \forall i,t, \tag{11d}$$

$$u_{i(t-1)} - u_{it} \le 1 - u_{i\tau_i^0}, \quad \forall i,t, \tag{11e}$$

$$y_{it} \ge u_{it} - u_{i(t-1)}, \quad \forall i,t, \tag{11f}$$

$$z_{it} \ge u_{i(t-1)} - u_{it}, \quad \forall i,t, \tag{11g}$$

$$\sum_{i\in\mathcal{I}_n}\left[r^+_{i\xi t} - r^-_{i\xi t} - p_{it}(1-\alpha_{i\xi t})\right] + \sum_{m:(n,m)\in\mathcal{L}} B_{nm}(\hat{\delta}_{nt} - \tilde{\delta}_{n\xi t} - \delta_{mt} + \tilde{\delta}_{m\xi t}) + \sum_{j\in\mathcal{J}_n}(W^*_{j\xi t} - w_{jt} - w^{\text{spill}}_{j\xi t}) + l^{\text{shed}}_{n\xi t} = 0, \quad \forall n,\xi,t, \tag{11h}$$

$$p_{it} + r^+_{i\xi t} \le \overline{P}_i u_{it}, \quad \forall i,\xi,t, \tag{11i}$$

$$p_{it} - r^-_{i\xi t} \ge \underline{P}_i u_{it}, \quad \forall i,\xi,t, \tag{11j}$$

$$p_{it} - p_{i(t-1)} + r^+_{i\xi t} - r^+_{i\xi(t-1)} \le R^{\text{U}}_i, \quad \forall i,\xi,t, \tag{11k}$$

$$p_{it} - p_{i(t-1)} - r^-_{i\xi t} + r^-_{i\xi(t-1)} \ge -R^{\text{D}}_i, \quad \forall i,\xi,t, \tag{11l}$$

$$r^+_{i\xi t} \le R^+_i \alpha_{i\xi t}, \quad \forall i,\xi,t, \tag{11m}$$

$$r^-_{i\xi t} \le R^-_i \alpha_{i\xi t}, \quad \forall i,\xi,t, \tag{11n}$$

$$B_{nm}(\hat{\delta}_{nt} - \hat{\delta}_{mt}) \le \overline{f}_{nm}, \quad \forall (n,m)\in\Lambda, t, \tag{11o}$$

$$w^{\text{spill}}_{j\xi t} \le w_{j\xi t}, \quad \forall j,\xi,t, \tag{11p}$$

$$l^{\text{shed}}_{n\xi t} \le D_{nt}, \quad \forall n,\xi,t, \tag{11q}$$

$$k_{i\xi t} = \frac{P_i K_i}{\sum_{i\in\mathcal{I}} P_i} u_{it}\alpha_{i\xi t}, \quad \forall i,\xi,t, \tag{11r}$$

$$F_{\xi t} = \sum_{i\in\mathcal{I}} \frac{F_i k_{i\xi t}}{R_i}, \quad \forall t,\xi, \tag{11s}$$

$$R_{\xi t} = \sum_{i\in\mathcal{I}} \frac{k_{i\xi t}}{R_i}, \quad \forall t,\xi, \tag{11t}$$

$$M_{\xi t} = \sum_{i\in\mathcal{I}} \frac{2H_i k_{i\xi t}}{K_i}, \quad \forall t,\xi, \tag{11u}$$

$$D_{\xi t} = \sum_{i\in\mathcal{I}} \frac{D_i k_{i\xi t}}{K_i}, \quad \forall t,\xi, \tag{11v}$$

$$\frac{\dot{f}_{\text{lim}}}{f_b}\frac{M_{\xi t}\sum_{i\in\mathcal{I}} P_i + M_v W_v}{\sum_{i\in\mathcal{I}} P_i + W_v} \ge \Delta P_{\xi t}, \quad \forall t,\xi, \tag{11w}$$

$$F_{\xi t} \ge F^{\text{lim}}_{\xi t},\ R_{\xi t} \ge R^{\text{lim}}_{\xi t}, \quad \forall t,\xi,$$

$$\frac{M_{\xi t}\sum_{i\in\mathcal{I}} P_i + M_v W_v}{\sum_{i\in\mathcal{I}} P_i + W_v} \ge M^{\text{lim}}_{\xi t}, \quad \forall t,\xi, \tag{11x}$$

$$\frac{D_{\xi t}\sum_{i\in\mathcal{I}} P_i + D_v W_v + R_d W_d}{\sum_{i\in\mathcal{I}} P_i + W_v + W_d} \ge D^{\text{lim}}_{\xi t}, \quad \forall t,\xi,$$

$$\frac{\Delta f_{\text{ss,lim}}}{f_0}\frac{D_{\xi t}\sum_{i\in\mathcal{I}} P_i + D_v W_v + R_d W_d}{\sum_{i\in\mathcal{I}} P_i + W_v + W_d} \ge \Delta P_{\xi t}, \quad \forall t,\xi, \tag{11y}$$

$$p_{it}\ge 0, \forall i,t;\ w_{jt}\ge 0, \forall j,t;\ \delta_{nt}\ge 0, \forall n,t;\ k_{i\xi t}, r^+_{i\xi t}, r^-_{i\xi t}\ge 0,$$

$$\forall i,\xi,t;\ \hat{\delta}_{n\xi t}, l^{\text{shed}}_{n\xi t}\ge 0, \forall n,\xi,t;\ w^{\text{spill}}_{j\xi t}\ge 0,\ \forall j,\xi,t;$$

$$F_{\xi t}, R_{\xi t}, M_{\xi t}, D_{\xi t}\ge 0, \forall \xi,t;\ u_{it}, y_{it}, z_{it}\in\{0,1\}, \tag{11z}$$

where $\Phi = \{p_{it},\ u_{it},\ y_{it},\ z_{it},\ \forall i,t;\ w_{jt}, \forall j,t;\ \delta_{nt}, \forall n,t;\ \hat{\delta}_{n\xi t}, \forall n,\xi,t; r^+_{i\xi t},\ r^-_{i\xi t}, \forall i,\xi,t;\ w^{\text{spill}}_{j\xi t}, \forall j,\xi,t;\ l^{\text{shed}}_{n\xi t},\ \forall n,\ \xi,t;\ \ k_{i\xi t},\ \forall i,\xi,t;\ F_{\xi t},\ R_{\xi t},\ M_{\xi t}, D_{\xi t}, \forall \xi,t\}$ represents the set of optimization variables.

The objective function (11a) to be minimized is the total expected system cost that comprises the day-ahead energy and the real-time balancing costs. The day-ahead component consists of the fuel costs C_i as well as the start-up and shut-down costs. The real-time component includes the re-dispatch cost from the deployment of upward and downward reserves based on the corresponding offer prices C_i^+ and C_i^-, as well as the involuntary load shedding at the value of lost load C^{sh}.

Equation (11b) enforces the nodal power balance of the day-ahead schedule, while network power flows at the day-ahead stage are restricted by the transmission capacity limits in (11c). Constraints (11d)-(11e) model the minimum online and offline time of conventional units based on commitment variable u_{it}, where parameters τ_i^1 and τ_i^0 are defined as $\tau_i^1 = \min\{t+T_i^1-1,\ T\}$ and $\tau_i^0 = \min\{t+T_i^0-1,\ T\}$, and T_i^1 and T_i^0 denote the duration that unit i should remain online and offline, respectively. Constraints (11f)-(11g) model the start-up and shut-down of conventional units using the binary variables y_{it} and z_{it}, respectively. The real-time power balance for every uncertainty realization ξ is enforced by constraint (11h). Parameter $\alpha_{i\xi t}$ models the availability of the generators to provide reserves, i.e., $\alpha_{i\xi t}$ is equal to 1 if generator i at scenario ξ and time t is online and able to provide reserves and zero otherwise. The scheduled energy production and the deployment of upward ($r^+_{i\xi t}$) and downward ($r^-_{i\xi t}$) reserves in each scenario ξ are bounded by the generation capacity limits of each unit by constraints (11i)-(11j), whereas constraints (11k)-(11l) enforce the upward and downward ramping limits accounting for the real-time reserve activation. Constraints (11m)-(11n) account for the limits of reserve capacity offers. Transmission capacity limits during real-time operation are enforced by constraint (11o), whereas wind spillage $w^{\text{spill}}_{j\xi t}$ and load shedding $l^{\text{shed}}_{n\xi t}$ are bounded by the wind power realization and the nodal demand through constraints (11p) and (11q), respectively.

The set of constraints (11r)-(11x) models the frequency limits of the power system. The equality constraint (11r) defines $k_{i\xi t}$ as the gain factor K_i of generator i scaled by the ratio of its capacity over the total system capacity, which in turn is multiplied by the

TABLE II
PARAMETERS OF THE THERMAL PLANTS AND VSM

Type	H_i [s]	K_i [p.u.]	F_i [p.u.]	R_i [p.u.]	D_i [p.u.]
Nuclear	4.5	0.98	0.25	0.04	0.6
CCGT	7.0	1.1	0.15	0.01	0.6
OCGT	5.5	0.95	0.35	0.03	0.6
VSM	6.0	1.0	-	-	0.6
Droop	-	1.0	-	0.05	-

binary variable u_{it} and the parameter $\alpha_{i\xi t}$ to indicate that a unit can provide inertial response only if it is committed and does not face an outage. Similarly, constraints (11s)-(11v) define average system variables for power fraction, droop, inertia and damping, respectively. Constraint (11w) enforces the RoCoF limit, while nadir equivalent and quasi steady-state frequency bounds are imposed by constraints (11x) and (11y). Finally, (11z) declares variables and provides trivial inequalities.

The main advantage of the stochastic UC model is its ability to endogenously define the reserve requirements and the number of conventional generators that should be committed at the day-ahead stage in order to contain real-time deviations of renewables and ensure sufficient frequency response in case of equipment outages. Therefore, the resulting generation schedule explicitly incorporates the frequency constraints, taking also into account the commitment status of synchronous generators.

VI. CASE STUDY

A. System Description

In order to analyze the performance of the stochastic UC model presented in Section V, a modified version of the IEEE RTS-96 power system from [25] is used, with 48 buses comprising areas 1 and 2 of the original system. Table II shows the relevant parameters of different thermal plant types, with H_i denoting the normalized inertia constant of the generators (i.e., $M_i = 2H_i$). The studied system includes 20 generators and 16 wind farms. It is assumed that six wind farms are providing virtual inertia; four of them via VSM control, and the remaining two through equivalent droop regulation. The UC is ran for two days without frequency constraints in order to initialize the system prior to introducing the frequency constraints on days 3, 4 and 5. This is done to ensure the impact of start-up costs is well distributed and not concentrated on one day. Therefore, the total simulation horizon is five days ($T = 120\,\mathrm{h}$), whereas the UC schedule is optimized separately for each day, with the last hour of each day used as an input for the next.

As the set of possible contingencies, the failure of synchronous generators $i = \{1, 6, 8, 10\}$ is considered. These generators are of various capacities, ranging from the smallest to the largest unit in the system. The hour 19 of day 3 (i.e., $t = 67\,\mathrm{h}$) is selected to be the time instance of a possible contingency, as this is the hour with high wind penetration and low demand. Wind power uncertainty is modelled using ten equiprobable scenarios that are provided in [25]. For further information on the scenario generation and reduction techniques that were applied to obtain this scenario set we refer the interested reader to [26]. Combining these wind power scenarios with the set of possible contingencies brings the total number of scenarios considered in the stochastic UC to 50. The optimization problem is formulated in Python and uses the Gurobi solver with default parameterization. All simulations were carried out using a laptop computer with Intel Core i7 CPU with a clock rate of 2.8 GHz and 16 GB of RAM.

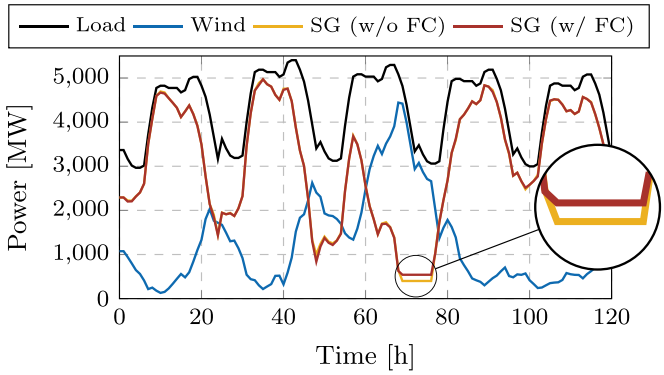

Fig. 5. UC dispatch of synchronous generation for respective load and wind profiles.

TABLE III
COMPARISON OF THE TOTAL NUMBER OF DISPATCHED GENERATORS THROUGH UC FOR EACH HOUR

Hour	65	66	67	68	69	70	71	72	73
w/o FC	6	5	4	4	4	4	4	4	4
w/ FC	6	5	10	10	10	10	10	10	10

B. Results

In this section, the simulation results from the stochastic UC are presented. Fig. 5 showcases the load and wind power profiles as well as the aggregate dispatch of synchronous generation for two UC runs: (i) without frequency constraints (denoted by w/o FC hereinafter); and (ii) with frequency constraints (denoted by w/ FC hereinafter). The simulation times for these two UC runs are 14 minutes 8 seconds and 14 minutes 28 seconds respectively, and thus the increase in computational time with the inclusion of frequency constraints can be considered marginal. Furthermore, Table III indicates the difference in the total number of generators committed between the two runs. Both Fig. 5 and Table III suggest that, although the amount of committed generators increases significantly, the total SG production is only slightly changed. This is because the extra generators are solely committed for the purpose of providing inertia, and are thus operating at their technical minimum. The production surplus arising from the additionally committed units is compensated by wind curtailment and other generators reducing their power output.

The evolution of aggregate system inertia over the course of the whole scheduling horizon is depicted in Fig. 6. A noticeable step change in total system inertia at hour 67 reflects the impact

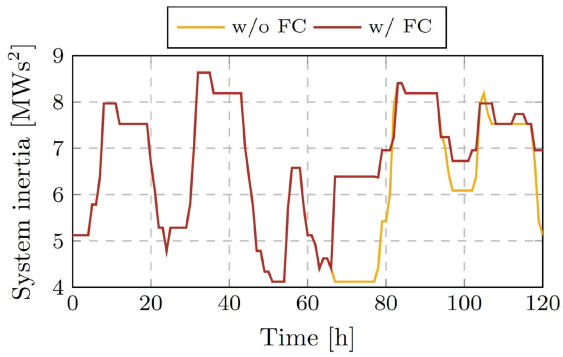

Fig. 6. Impact of frequency constraints on the aggregate level of system inertia.

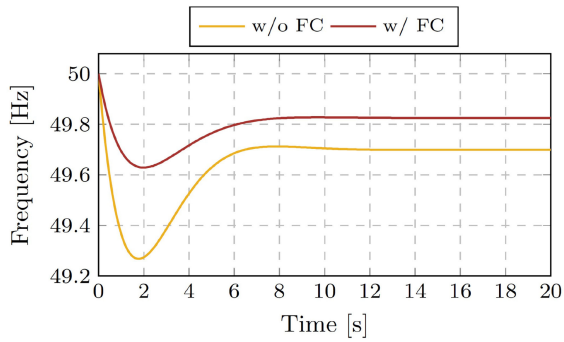

Fig. 8. Frequency evolution of the CoI with and without FC for 20 seconds after the fault instance at $t = 67$ h.

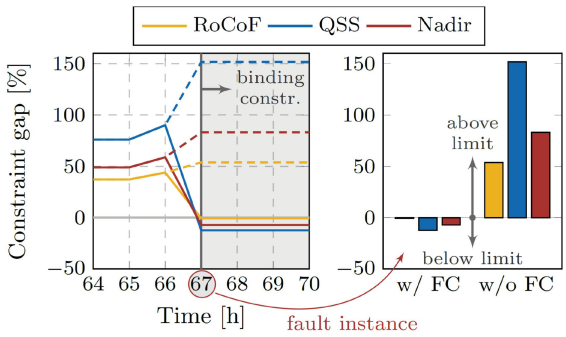

Fig. 7. Constraint gaps for different frequency metrics. Dashed lines refer to the case without frequency constraints.

of frequency constraints under contingency, which subsequently trigger a dispatch of auxiliary synchronous generators. While the inertia levels do not differentiate between the two cases during the first two days, on the days following the potential outage some carryover impacts can be observed. This is a consequence of the commitment schedule being radically changed at hour $t = 67$, thus affecting the UC schedules in the following days.

Some insightful conclusions can be drawn from Fig. 7, where the difference between the actual values of the frequency metrics and the respective ENTSO-E thresholds are depicted. For this purpose, we define a constraint gap ϵ as a measure of the relative constraint distance to its limit, e.g., $\epsilon_{\text{nadir}} = \Delta f_{\max}/\Delta f_{\lim} - 1$. After the completion of unit commitment, the constraints are re-evaluated using the obtained F_g, R_g and M values in order to determine which frequency criterion becomes binding at the instance of the fault. A negative constraint gap indicates that the specific frequency criteria is met with room to spare. It should be noted that the positive values of ϵ for $t < 67$ h indicate that the frequency threshold would be violated if a fault occurs. No action is required however, considering that in this case study we assume that the contingency can only occur at hour $t = 67$. Fig. 7 demonstrates that without explicit consideration of frequency-related constraints in the stochastic UC model all prescribed frequency limits would be violated. Moreover, it can be observed that when taking such constraints into account, the RoCoF constraint is closest to its limit - corresponding to the smallest constraint gap - and thus binding. The constraint

TABLE IV
UNIT COMMITMENT COSTS [$] BREAKDOWN ON DAY 3

Case	Total costs	Start-up	Operation	Reserves
w/o FC	410 545	788	405 561	4 196
w/ FC	432 383	2 248	420 886	9 249
Difference	5.32 %	185 %	3.78 %	120 %

gap difference between the two cases at hour $t = 67$ clearly highlights the importance of including the frequency constraints in UC in order to avoid large frequency excursions and undesired triggering of protection and UFLS schemes. The same observations are also reflected in Fig. 8 through representation of the time-domain frequency response of the system following a disturbance. Understandably, the values of RoCoF, nadir and steady-state deviation are reduced compared to the case without frequency constraints, such that all of the ENTSO-E criteria are fulfilled.

Finally, the economic impact of including the frequency constraints into the stochastic UC model is investigated. The breakdown of operational costs for day 3 is presented in Table IV. The addition of frequency constraints leads to a 5 % increase in total expected system costs and a significant increase in start-up costs by 185 %. This is due to six extra generators being turned on for providing inertia at the period of a potential generation failure, as shown in Table III. A large increase is also seen in reserve scheduling costs, as the reserves are now not only scheduled to cover wind power uncertainty but also for possible contingencies. The change in cost is of course highly dependent on the specific system and the considered contingencies.

VII. CONCLUSION

This paper includes frequency constraints in the UC problem of a system with large wind power penetration in order to investigate the impact of frequency dynamics on unit scheduling. By employing the analytic expressions for post-contingency frequency response of a multi-machine system, a set of constraints reflecting the frequency nadir, RoCoF and quasi steady-state deviation is defined. The highly non-linear frequency nadir constraint is linearized using two approaches: (i) a PWL technique adapted from the literature; and (ii) a proposed simple and

efficient method for extracting bounds on decision variables of interest, which is shown to be computationally superior to PWL. Using the latter approach, the stochastic UC problem is formulated as an MILP, with an objective of minimizing the expected system costs against wind power production and generation outage uncertainties.

Our results show that the inclusion of frequency constraints in the UC model significantly affects the dispatch of synchronous generators and consequently the expected system costs. In particular, during anticipated critical events such as the loss of generation, additional synchronous machines are needed for providing sufficient inertia and damping in the process of frequency containment. Such actions lead to a drastic increase in the UC costs, especially pertaining to start-up and reserve scheduling, which poses a new challenge as the operator must find a way to remunerate the units committed for the sole purpose of frequency regulation. This is an exciting avenue for future work.

For clarity, here we present in more detail the mathematical formulation of how the PWL optimization problem in (6) is solved. With $\nu = 4$, the inner $\max$ operator from the objective function in (6) can be eliminated by defining the following terms:

$$t_3 = \max\{t_2,\, a_4 R_g^{(\eta)} + b_4 F_g^{(\eta)} + c_4 M^{(\eta)} + d_4\}, \tag{12a}$$

$$t_2 = \max\{t_1,\, a_3 R_g^{(\eta)} + b_3 F_g^{(\eta)} + c_3 M^{(\eta)} + d_3\}, \tag{12b}$$

$$t_1 = \max\{a_2 R_g^{(\eta)} + b_2 F_g^{(\eta)} + c_2 M^{(\eta)} + d_2,\; a_1 R_g^{(\eta)} + b_1 F_g^{(\eta)} + c_1 M^{(\eta)} + d_1\}. \tag{12c}$$

Subsequently, the complete optimization problem in (6) is reformulated as

$$\min_{\Psi} \sum_{\eta} \left(t_3 \left(R_g^{(\eta)}, F_g^{(\eta)}, M^{(\eta)} \right) - \Delta f_{\max} \left(R_g^{(\eta)}, F_g^{(\eta)}, M^{(\eta)} \right) \right)^2 \tag{13}$$

subject to

$$a_1 R_g^{(\eta)} + b_1 F_g^{(\eta)} + c_1 M^{(\eta)} + d_1 \le t_1 \le a_1 R_g^{(\eta)} + b_1 F_g^{(\eta)} + c_1 M^{(\eta)} + d_1 + v_1 A \quad \forall \eta, \tag{14a}$$

$$a_2 R_g^{(\eta)} + b_2 F_g^{(\eta)} + c_2 M^{(\eta)} + d_2 \le t_1 \le a_2 R_g^{(\eta)} + b_2 F_g^{(\eta)} + c_2 M^{(\eta)} + d_2 + (1 - v_1) A \quad \forall \eta, \tag{14b}$$

$$t_1 \le t_2 \le t_1 + v_2 A \quad \forall \eta, \tag{14c}$$

$$a_3 R_g^{(\eta)} + b_3 F_g^{(\eta)} + c_3 M^{(\eta)} + d_3 \le t_2 \le a_3 R_g^{(\eta)} + b_3 F_g^{(\eta)} + c_3 M^{(\eta)} + d_3 + (1 - v_2) A \quad \forall \eta, \tag{14d}$$

$$t_2 \le t_3 \le t_2 + v_3 A \quad \forall \eta, \tag{14e}$$

$$a_4 R_g^{(\eta)} + b_4 F_g^{(\eta)} + c_4 M^{(\eta)} + d_4 \le t_3 \le a_4 R_g^{(\eta)} + b_4 F_g^{(\eta)} + c_4 M^{(\eta)} + d_4 + (1 - v_3) A \quad \forall \eta, \tag{14f}$$

where v_1, v_2, v_3 are binary variables and A is a sufficiently large scalar.

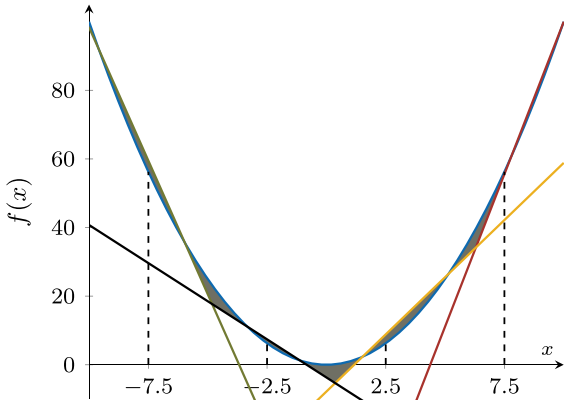

Fig. 9. Illustration of the PWL method on a 2-D function.

We visually illustrate with a simple 2-D example in Fig. 9 how the PWL optimization problem from (13) is solved. There are four evaluation points set at -7.5, -2.5, 2.5 and 7.5, and the respective function is approximated with four segments. At each evaluation point the model identifies the segment closest to the original curve, and subsequently aims to minimize the overall shaded area. The proposed technique can then be expanded and employed on a function of three variables, as we have done with the expression for frequency nadir.

REFERENCES

[1] F. Milano, F. Dörfler, G. Hug, D. J. Hill, and G. Verbič, "Foundations and challenges of low-inertia systems," in *Proc. Power Syst. Comput. Conf.*, Jun. 2018, pp. 1–25.

[2] P. Tielens and D. Van Hertem, "Grid inertia and frequency control in power systems with high penetration of renewables," in *Proc. Young Researchers Symp. Elect. Power Eng.*, 2012.

[3] J. Matevosyan and P. Du, "Wind integration in ERCOT," in *Integration of Large-Scale Renewable Energy into Bulk Power Systems*. Berlin, Germany: Springer, 2017, pp. 1–25.

[4] EirGrid and SONI, "DS3 System Services: Review TSO Recommendations," EirGrid, Dublin, Ireland, Tech. Rep., May 2013.

[5] EirGrid and SONI, "DS3 System Services: Portfolio Capability Analysis," , EirGrid, Dublin, Ireland, Tech. Rep., Nov 2014.

[6] E. Davarinejad, M. R. Hesamzadeh, and H. Chavez, "Incorporating inertia constraints into the power market," Energiforsk, Stockholm, Sweden, Tech. Rep., 2017.

[7] F. Pérez-Illanes, E. Álvarez-Miranda, C. Rahmann, and C. Campos-Valdés, "Robust unit commitment including frequency stability constraints," *Energies*, vol. 9, no. 11, p. 957–972, 2016.

[8] P. Daly, D. Flynn, and N. Cunniffe, "Inertia considerations within unit commitment and economic dispatch for systems with high non-synchronous penetrations," in *Proc. IEEE Eindhoven PowerTech*, 2015, pp. 1–6.

[9] H. Ahmadi and H. Ghasemi, "Security-constrained unit commitment with linearized system frequency limit constraints," *IEEE Trans. Power Syst.*, vol. 29, no. 4, pp. 1536–1545, Jul. 2014.

[10] F. Teng, V. Trovato, and G. Strbac, "Stochastic scheduling with inertia-dependent fast frequency response requirements," *IEEE Trans. Power Syst.*, vol. 31, no. 2, pp. 1557–1566, Mar. 2016.

[11] L. Badesa, F. Teng, and G. Strbac, "Optimal scheduling of frequency services considering a variable largest-power-infeed-loss," in *Proc. IEEE Power Energy Soc. General Meet.*, Aug. 2018, pp. 1–5.

[12] M. Brito, E. Gil, and I. Calle, "Unit commitment with primary frequency control requirements for low-inertia systems," in *Proc. IEEE Power Energy Soc. General Meet.*, Aug. 2018, pp. 1–5.

[13] V. Trovato, A. Bialecki, and A. Dallagi, "Unit commitment with inertia-dependent and multispeed allocation of frequency response services," *IEEE Trans. Power Syst.*, vol. 34, no. 2, pp. 1537–1548, Mar. 2019.

[14] D. Lee Hau Aik, "A general-order system frequency response model incorporating load shedding: Analytic modeling and applications," *IEEE Trans. Power Syst.*, vol. 21, no. 2, pp. 709–717, May 2006.
[15] U. Markovic, Z. Chu, P. Aristidou, and G. Hug, "LQR-based Adaptive virtual synchronous machine for power systems with high inverter penetration," *IEEE Trans. Sustain. Energy*, vol. 10, no. 3, pp. 1501–1512, Jul. 2019.
[16] P. M. Anderson and M. Mirheydar, "A low-order system frequency response model," *IEEE Trans. Power Syst.*, vol. 5, no. 3, pp. 720–729, Aug. 1990.
[17] J. Rocabert, A. Luna, F. Blaabjerg, and P. Rodrguez, "Control of power converters in AC microgrids," *IEEE Trans. Power Electron.*, vol. 27, no. 11, pp. 4734–4749, Nov. 2012.
[18] U. Markovic, O. Stanojev, P. Aristidou, and G. Hug, "Partial grid forming concept for 100% inverter-based transmission systems," in *Proc. IEEE Power Energy Soc. General Meet.*, Aug. 2018, pp. 1–5.
[19] U. Tamrakar, D. Shrestha, M. Manisha, B. P. Bhattarai, T. M. Hansen, and R. Tonkoski, *Virtual Inertia: Current Trends and Future Directions*. Basel, Switzerland: MDPI AG, Jun. 2017.
[20] ENTSO-E, "Frequency stability evaluation criteria for the synchronous zone of continental europe," , ENTSO-E, Brussels, Belgium, Tech. Rep., 2016.
[21] A. Ahmadi-Khatir, A. J. Conejo, and R. Cherkaoui, "Multi-area energy and reserve dispatch under wind uncertainty and equipment failures," *IEEE Trans. Power Syst.*, vol. 28, no. 4, pp. 4373–4383, Nov. 2013.
[22] R. N. Allan and R. Billinton, *Reliability Evaluation of Power Systems*. Berlin, Germany: Springer, 2013.
[23] A. J. Conejo, M. Carrión, and J. M. Morales, *Decision Making Under Uncertainty in Electricity Markets*, vol. 1, Berlin, Germany: Springer, 2010.
[24] S. Delikaraoglou and P. Pinson, "High-quality wind power scenario forecasts for decision-making under uncertainty in power systems," in *Proc. 13th IEEE Int. Workshop Large-Scale Integration Wind Power Transmiss. Netw.*, 2014.
[25] H. Pandzic, Y. Dvorkin, T. Qiu, Y. Wang, and D. Kirschen, Unit Commitment under Uncertainty - GAMS Models, Library of the Renewable Energy Analysis Lab (REAL), University of Washington, Seattle, USA. [Online]. Available at: http://www.ee.washington.edu/research/real/gams_code.html.
[26] Y. Dvorkin, H. Pandžić, M. A. Ortega-Vazquez, and D. S. Kirschen, "A hybrid stochastic/interval approach to transmission-constrained unit commitment," *IEEE Trans. Power Syst.*, vol. 30, no. 2, pp. 621–631, Mar. 2014.

Matthieu Paturet received the M.Sc. degree in energy science and technology from the Swiss Federal Institute of Technology, Zurich, Switzerland, in 2019. He is currently working as an Energy Data Analyst at Zeigo in London, UK. His research interests include electricity markets and optimization of power systems.

Uros Markovic (Member, IEEE) was born in Belgrade, Serbia. He received the Dipl.-Eng. degree in electrical engineering from the University of Belgrade, Serbia, in 2013, with a major in power systems. He received the M.Sc. and Ph.D. degrees in electrical engineering and information technology in 2016 and 2020, respectively, both from the Swiss Federal Institute of Technology (ETH), Zurich, Switzerland. He is currently a joint Postdoctoral Researcher with the Power Systems Laboratory and the Automatic Control Laboratory of ETH Zurich, Switzerland, and an affiliated Researcher at the Grid Integration Group (GIG) of Lawrence Berkeley National Laboratory (LBNL), California, USA.

His research interests include power system dynamics, control and optimization, with a focus on stability and operation of inverter-dominated power systems with low rotational inertia.

Stefanos Delikaraoglou (Member, IEEE) received the Dipl.-Eng. degree from the School of Mechanical Engineering, National Technical University of Athens, Greece, in 2010 and the M.Sc. degree in sustainable energy from the Technical University of Denmark in 2012. He holds a Ph.D. degree awarded in 2016 by the Department of Electrical Engineering at the Technical University of Denmark. From 2017 to 2019, he was a Postdoctoral Researcher with the Power Systems Laboratory at the Swiss Federal Institute of Technology (ETH), Zurich, Switzerland, and he is currently a Postdoctoral Associate with the Laboratory for Information and Decision Systems (LIDS), Massachusetts Institute of Technology (MIT), MA, USA.

His research interests include energy markets and multi-energy systems modeling, decision-making under uncertainty, equilibrium models and hierarchical optimization.

Evangelos Vrettos (Member, IEEE) received the Dipl.-Ing degree in electrical and computer engineering from the National Technical University of Athens, Greece, in 2010, with a major in power systems. He joined the Power Systems Laboratory (PSL) at the Swiss Federal Institute of Technology (ETH), Zurich, Switzerland, in 2011, where he received the Ph.D. degree in electrical engineering and information technology in 2016, and continued as a Postdoctoral Researcher for half a year. He is currently an R&D Manager at Swissgrid, the Swiss electricity transmission system operator, and an Affiliated Researcher at the Grid Integration Group (GIG) of Lawrence Berkeley National Laboratory (LBNL), California, USA.

His research has focused on optimization and control for demand response and energy storage resources, low-inertia power systems and, more recently, optimal power flow applications for congestion management and blockchain-based solutions for ancillary services markets.

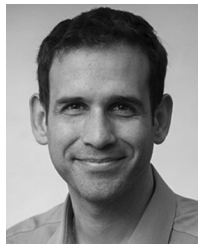

Petros Aristidou (Senior Member, IEEE) received a Diploma in electrical and computer engineering from the National Technical University of Athens, Greece, in 2010, and a Ph.D. degree in engineering sciences from the University of Liège, Belgium, in 2015. He is currently a Lecturer in sustainable power systems at the Cyprus University of Technology. His research interests include power system dynamics, control, and simulation.

Gabriela Hug (Senior Member, IEEE) was born in Baden, Switzerland. She received the M.Sc. degree in electrical engineering in 2004 and the Ph.D. degree in 2008, both from the Swiss Federal Institute of Technology (ETH), Zurich, Switzerland. After the Ph.D. degree, she worked in the Special Studies Group of Hydro One, Toronto, ON, Canada, and from 2009 to 2015, she was an Assistant Professor in Carnegie Mellon University, Pittsburgh, PA, USA. She is currently an Associate Professor in the Power Systems Laboratory, ETH Zurich. Her research is dedicated to control and optimization of electric power systems.